

# Radiation pressure of light pulses and conservation of linear momentum in dispersive media

Michael Scalora,<sup>1</sup> Giuseppe D'Aguanno,<sup>1</sup> Nadia Mattiucci,<sup>2,1</sup> Mark J. Bloemer,<sup>1</sup> Marco Centini,<sup>3</sup>  
Concita Sibilìa,<sup>3</sup> and Joseph W. Haus<sup>4</sup>

<sup>1</sup>*Charles M. Bowden Research Center, AMSRD-AMR-WS-ST, Research, Development, and Engineering Center,  
Redstone Arsenal, Alabama 35898-5000, USA*

<sup>2</sup>*Time Domain Corporation, Cummings Research Park, 7057 Old Madison Pike, Huntsville, Alabama 35806, USA*

<sup>3</sup>*INFN at Dipartimento di Energetica, Università di Roma "La Sapienza", Via A. Scarpa 16, 00161 Roma, Italy*

<sup>4</sup>*Electro-Optics Program, University of Dayton, Dayton, Ohio 45469-0245, USA*

(Received 12 December 2005; revised manuscript received 1 March 2006; published 16 May 2006)

We derive an expression for the Minkowski momentum under conditions of dispersive susceptibility and permeability, and compare it to the Abraham momentum in order to test the principle of conservation of linear momentum when matter is present. We investigate cases when an incident pulse interacts with a variety of structures, including thick substrates, resonant, free-standing, micron-sized multilayer stacks, and negative index materials. In general, we find that for media only a few wavelengths thick the Minkowski and Abraham momentum densities yield similar results. For more extended media, including substrates and Bragg mirrors embedded inside thick dielectric substrates, our calculations show dramatic differences between the Minkowski and Abraham momenta. Without exception, in all cases investigated the instantaneous Lorentz force exerted on the medium is consistent only with the rate of change of the Abraham momentum. As a practical example, we use our model to predict that electromagnetic momentum and energy buildup inside a multilayer stack can lead to widely tunable accelerations that may easily reach and exceed  $10^{10}$  m/s<sup>2</sup> for a mass of  $10^{-5}$  g. Our results suggest that the physics of the photonic band edge and other similar finite structures may be used as a testing ground for basic electromagnetic phenomena such as momentum transfer to macroscopic media.

DOI: [10.1103/PhysRevE.73.056604](https://doi.org/10.1103/PhysRevE.73.056604)

PACS number(s): 42.25.Bs, 42.25.Gy, 42.70.Qs, 78.20.Ci

## I. INTRODUCTION

For the better part of two decades photonic band gap (PBG) structures have been the subject of many theoretical and experimental studies. Since the pioneering work of Yablonoitch [1] and John [2], investigations have focused on all kinds of geometrical arrangements, which vary from one-dimensional, layered stacks, more amenable to analytical treatment, to much more complicated three-dimensional topologies that require a full vector Maxwell approach [3]. In our current effort, in part we focus our attention on a different aspect of this particular problem, namely the interaction of short pulses with free-standing, resonant structures interacting with pulses of finite bandwidth. Interesting questions arise as incident pulses are tuned near the band edge, where electromagnetic energy and momentum become temporarily stored inside the medium. When tuned near the band edge, in the absence of meaningful absorption, a pulse of finite bandwidth can lose forward momentum in at least two ways: (i) by tuning inside the gap, which results in mirrorlike reflections and maximum transfer of momentum and (ii) by tuning at a band edge resonance, where the transfer of momentum is a minimum, and the field becomes localized inside the stack. It has been shown that relatively narrow-band optical pulses may be transmitted without scattering losses or shape changes [4], insuring that momentum and energy storage inside the structure is only temporary. Therefore, a structure not fixed to the laboratory frame naturally acquires linear momentum in an effort to conserve it. In what follows we attempt to answer the following question: how much and what sort of motion results from the interaction?

The issue of radiation pressure on macroscopic bodies arches all the way back to Maxwell [5], who realized that

light in fact exerts pressure, and was later experimentally verified by Nichols and Hull [6]. A good perspective of the early history of the subject is given by Mulser [7], who also showed that resonant multiwave interactions, such as stimulated Brillouin and Raman scattering, are radiation-pressure-driven phenomena. More recently, Antonoyiannakis and Pendry [8] examined issues related to forces present in photonic crystals and found that when traversing from a low to a high dielectric material, a light beam attracts the interface. The implications then extend to 3D (three-dimensional) photonic crystals, and the authors go on to predict an attractive force between neighboring dielectric spheres. Povinelli *et al.* [9] studied the effects of radiation pressure in omnidirectional reflector waveguides. They showed that as light propagates down the guide (parallel to the dielectric mirrors), radiation pressure causes the mirrors to attract, and, in the absence of any losses, the attractive force appears to diverge near the cut off frequency. Tucker *et al.* [10] have investigated effects of radiation pressure and thermal jitter in a hybrid environment, composed of a Fabry-Perot resonator as part of a micromechanical switching mechanism (MEMS). The authors found that radiation pressure can cause small changes in the separation of movable mirrors even at room temperature, leading to nonlinear shifts of the Fabry-Perot resonance and hysteresis loops. In MEMS lasers, the authors suggest that nonlinear radiation pressure effects may induce changes in the characteristic low-frequency chirp of the device [10].

The issue of how much electromagnetic momentum is transferred to macroscopic bodies is still a matter of debate, primarily "...because what is considered electromagnetic and what mechanical is to some extent arbitrary..." as noted by Jackson [11]. There are two well-known expressions that

one may use, one due to Minkowski [12], the other perhaps more familiar form due to Abraham [13]. The latter is generally believed to be the correct expression, even though the Minkowski form follows from momentum conservation arguments in the presence of matter, beginning with Maxwell's equations and the Lorentz force [11]. Nevertheless, the subject has been controversial, and the Minkowski expression is believed to be flawed, in part because it is connected to a stress-energy tensor that forces both the susceptibility and permeability to be independent of density and temperature [11], an unphysical situation that argues against it.

Our approach does not include the formulation of a stress-energy tensor, as is often done [8,9,14], for example, because that may tend to obscure the problem rather than clarify it, while providing no more definitive answers one way or the other. In order to remove some of the ambiguities inherent in the definition of a stress-tensor, which has some degree of built-in arbitrariness, one may address the problem by directly integrating the vector Maxwell's equations in space and time in the presence of matter, using pulses of finite extent to include material dispersion and finite response times, and by treating more realistic extended structures of finite length. The resulting fields may then be used to form various quantities of interest, such as the Lorentz force [15,16], for example, so that a direct assessment may be made regarding momentum conservation. In Ref. [15], for example, using a quantum mechanical approach, Loudon showed that beginning with a Lorentz force density in ordinary materials ( $\mu=1$ ), in the absence of free charges and currents,

$$\mathbf{f}(\mathbf{r},t) = \frac{1}{c} \frac{\partial \mathbf{P}}{\partial t} \times \mathbf{B}, \quad (1)$$

the momentum a photon delivers to a surface when incident from free space when absorption is absent is [15]

$$P_T = 2P_0 \frac{n-1}{n+1}, \quad (2)$$

where  $n$  is the index of the material and  $P_0$  is the initial momentum. Recently, Mansuripur [16] suggested that based on his calculation of momentum transfer to a transparent slab via the application of boundary conditions, the most plausible definition of momentum density is neither the Abraham nor the Minkowski momentum, rather, an average of the two momentum densities combined into a simple, symmetrized form [16]:

$$\mathbf{g}_{average} = \frac{1}{4\pi c} \left( \frac{(\mathbf{D} \times \mathbf{B})_{\text{Minkowski}} + (\mathbf{E} + \mathbf{H})_{\text{Abraham}}}{2} \right). \quad (3)$$

Assuming the usual constitutive relation  $\mathbf{D} = \mathbf{E} + 4\pi\mathbf{P}$ , the absence of dispersion, and that  $\mu=1$ , it is easy to show that Eq. (3) reduces to [16]

$$\mathbf{g}_{average} = \left( \frac{\mathbf{P} \times \mathbf{H}}{2c} + \frac{\mathbf{E} \times \mathbf{H}}{4\pi c} \right). \quad (4)$$

One may easily identify the second term on the right-hand side as the usual Abraham electromagnetic momentum density. The first term on the right-hand side of Eq. (4) is asso-

ciated with the (apparently) mechanical momentum [13,17] of the bound charges moving within the dielectric material.

In earlier work, Gordon [18] had shown that in a low-density gas the Lorentz force density may be recast as

$$\mathbf{f}(\mathbf{r},t) = \alpha \left[ \nabla \left( \frac{1}{2} E^2 \right) + \frac{1}{c} \frac{\partial}{\partial t} (\mathbf{E} \times \mathbf{H}) \right], \quad (5)$$

where  $\alpha$  is the medium's polarizability. The author went on to apply Eq. (5) to the case of radiation reflected from a perfect conductor. Integrating over all volume, with the requirement that the field go to zero at the conductor's surface (this condition is also valid for well-localized wave packets, whose boundary conditions are zero at infinity), the first term on the right-hand side vanishes, and the sole contribution to the total force is

$$\mathbf{F}(t) = \frac{N\alpha}{c} \int_{\text{volume}} dv \frac{\partial}{\partial t} (\mathbf{E} \times \mathbf{H}), \quad (6)$$

where  $N$  is the particle density.

In the present work we derive expressions for the Minkowski momentum density and for the Lorentz force density in the general case of dispersive  $\epsilon$  and  $\mu$ , and study the interaction of short optical pulses incident on (i) dielectric substrates of finite length, (ii) micron-sized, multilayer structures located in free space and also embedded within a dielectric medium, and (iii) a negative index material (NIM), a medium that simultaneously displays negative  $\epsilon$  and  $\mu$  [19]. Integrating the vector Maxwell equations in two-dimensional space and time, in all cases that we investigate we find that *conservation of linear momentum and the Lorentz force are consistent only with the temporal rate of change of the Abraham momentum, regardless of the medium and its dispersive properties, in regions of negligible absorption, namely,*

$$\frac{\partial}{\partial t} \left( \mathbf{P}_{mech} + \int_{\text{ALL VOLUME}} \frac{\mathbf{E} \times \mathbf{H}}{4\pi c} dv \right) = \mathbf{0}, \quad (7)$$

where  $\mathbf{F}(t) = \frac{\partial \mathbf{P}_{mech}}{\partial t}$  is the instantaneous Lorentz force. Thus, even though they may be related to the Abraham momentum, neither the Minkowski nor the average momentum density in Eq. (3) above, or any other plausible definition, are capable of reproducing the Lorentz force in any of the circumstances investigated. They come close in situations where the size of the structure is much smaller compared to the spatial extension of the incident wave packet, or if reflections occur from a mirror located in free space. In these cases the analysis of the dynamics reveals only transient, relatively small differences.

Once we establish the theoretical basis of our approach, we go on to examine the response of relatively thick substrates and micron-sized resonant structures, and then the response of extended, NIM substrates, illuminated by pulses several tens of wave cycles in duration. Under some circumstances, the spatial extension of the pulse may be several tens of microns, which is much longer than the length of any typical multilayer structure [4]. Although the theoretical approach that we develop will apply to pulses of arbitrary du-

ration, the typical situation that we describe may be compared to a scattering event, during which most of the pulse is located outside the structure. The consequence of this is that the Minkowski and the Abraham momentum densities display only small differences that decrease as pulse width is increased (the medium contribution in Eq. (4) above is limited by the small spatial extension of the structure compared to spatial pulse width). In the current situation we compare the two expressions of momentum density because, unlike the simpler Abraham expression, unusual conditions could intervene to significantly alter the appearance and substance of the Minkowski momentum density in a way that depends on the nature of the medium and its dispersive properties, thus creating circumstances that may help discriminate between the two quantities even in the transient regime. With these considerations in mind, we set out to derive generalized forms of the momentum densities, and a generalized Lorentz force density under conditions of dispersive  $\varepsilon$  and  $\mu$ , with an eye also toward applications to NIMs [19], which we briefly treat later in the manuscript.

## II. THE MODEL

We use the Gaussian system of units, and for the moment we assume a TE-polarized incident field of the form

$$\begin{aligned}\mathbf{E} &= \hat{\mathbf{x}}(\mathcal{E}_x(y, z, t)e^{i(k_z z - k_y y - \omega_0 t)} + \text{c.c.}), \\ \mathbf{H} &= \hat{\mathbf{y}}(\mathcal{H}_y(y, z, t)e^{i(k_z z - k_y y - \omega_0 t)} + \text{c.c.}) \\ &\quad + \hat{\mathbf{z}}(\mathcal{H}_z(y, z, t)e^{i(k_z z - k_y y - \omega_0 t)} + \text{c.c.}),\end{aligned}\quad (8)$$

where  $\hat{\mathbf{x}}, \hat{\mathbf{y}}, \hat{\mathbf{z}}$  are the unit directional vectors;  $\mathbf{E}$  and  $\mathbf{H}$  are real electric and magnetic fields, respectively;  $\mathcal{E}_x(y, z, t)$ ,  $\mathcal{H}_y(y, z, t)$ , and  $\mathcal{H}_z(y, z, t)$  are general, complex envelope functions; and  $k_z = |\mathbf{k}| \cos \theta_i$  and  $k_y = -|\mathbf{k}| \sin \theta_i$ ,  $|\mathbf{k}| = k_0 = \omega_0 / c$ . This choice of carrier wave vector is consistent with a pulse initially located in vacuum. We make no other assumptions about the envelope functions. The model that we adopt takes material dispersion (including absorption) into account and makes virtually no approximations. Following Eqs. (8), the displacement field  $\mathbf{D}$  may be similarly defined as follows:  $\mathbf{D} = \hat{\mathbf{x}}(\mathcal{D}_x(y, z, t)e^{i(k_z z - k_y y - \omega_0 t)} + \text{c.c.})$ , and may be related to the electric field by expanding the complex dielectric function as a Taylor series in the usual way:

$$\begin{aligned}\varepsilon(\mathbf{r}, \omega) &= \varepsilon(\mathbf{r}, \omega_0) + \left. \frac{\partial \varepsilon(\mathbf{r}, \omega)}{\partial \omega} \right|_{\omega_0} (\omega - \omega_0) \\ &\quad + \frac{1}{2} \left. \frac{\partial^2 \varepsilon(\mathbf{r}, \omega)}{\partial \omega^2} \right|_{\omega_0} (\omega - \omega_0)^2 + \dots \\ &= a(\mathbf{r}, \omega_0) + b(\mathbf{r}, \omega_0)\omega + c(\mathbf{r}, \omega_0)\omega^2 + \dots.\end{aligned}\quad (9)$$

Then, for an isotropic medium, a simple constitutive relation may be written as follows:

$$\begin{aligned}\mathcal{D}_x(\mathbf{r}, t) &= \int_{-\infty}^{\infty} \varepsilon(\mathbf{r}, \omega) \tilde{\mathcal{E}}_x(\mathbf{r}, \omega) e^{-i\omega t} d\omega \\ &= \int_{-\infty}^{\infty} [a(\mathbf{r}, \omega_0) + b(\mathbf{r}, \omega_0)\omega + c(\mathbf{r}, \omega_0)\omega^2 + \dots] \\ &\quad \times [\tilde{\mathcal{E}}_x(\mathbf{r}, \omega)] e^{-i\omega t} d\omega,\end{aligned}\quad (10)$$

where  $\tilde{\mathcal{E}}_x(\mathbf{r}, \omega)$  is the Fourier transform of  $\mathcal{E}_x(\mathbf{r}, t)$ . Assuming that a similar development follows for the magnetic fields, it is easy to show that

$$\begin{aligned}\mathcal{D}_x(\mathbf{r}, t) &= \varepsilon(\mathbf{r}, \omega_0) \mathcal{E}_x(\mathbf{r}, t) + i \frac{\partial \varepsilon(\mathbf{r}, \omega_0)}{\partial \omega} \frac{\partial \mathcal{E}_x(\mathbf{r}, t)}{\partial t} + \dots, \\ \mathcal{B}_y(\mathbf{r}, t) &= \mu(\mathbf{r}, \omega_0) \mathcal{H}_y(\mathbf{r}, t) + i \frac{\partial \mu(\mathbf{r}, \omega_0)}{\partial \omega} \frac{\partial \mathcal{H}_y(\mathbf{r}, t)}{\partial t} + \dots, \\ \mathcal{B}_z(\mathbf{r}, t) &= \mu(\mathbf{r}, \omega_0) \mathcal{H}_z(\mathbf{r}, t) + i \frac{\partial \mu(\mathbf{r}, \omega_0)}{\partial \omega} \frac{\partial \mathcal{H}_z(\mathbf{r}, t)}{\partial t} + \dots.\end{aligned}\quad (11)$$

We emphasize that the field decomposition that highlights an envelope function and a carrier frequency is done as a matter of convenience and should be viewed as a simple mathematical transformation because the field retains its generality. Substituting Eqs. (11) into the definition of the Minkowski momentum density we find

$$\begin{aligned}\mathbf{g}_{Minkowski} &= \frac{\mathbf{D} \times \mathbf{B}}{4\pi c} = \frac{1}{4\pi c} \hat{\mathbf{z}} \left\{ [\varepsilon(\omega_0) \mu^*(\omega_0) \mathcal{E}_x \mathcal{H}_y^* + \text{c.c.}] \right. \\ &\quad + \left( i \varepsilon^*(\omega_0) \frac{\partial \mu(\omega_0)}{\partial \omega} \mathcal{E}_x^* \frac{\partial \mathcal{H}_y}{\partial t} + \text{c.c.} \right) \\ &\quad + \left( i \mu^*(\omega_0) \frac{\partial \varepsilon(\omega_0)}{\partial \omega} \mathcal{H}_y^* \frac{\partial \mathcal{E}_x}{\partial t} + \text{c.c.} \right) + \dots \left. \right\} \\ &\quad - \frac{1}{4\pi c} \hat{\mathbf{y}} \left\{ [\varepsilon(\omega_0) \mu^*(\omega_0) \mathcal{E}_x \mathcal{H}_z^* + \text{c.c.}] \right. \\ &\quad + \left( i \varepsilon^*(\omega_0) \frac{\partial \mu(\omega_0)}{\partial \omega} \mathcal{E}_x^* \frac{\partial \mathcal{H}_z}{\partial t} + \text{c.c.} \right) \\ &\quad + \left( i \mu^*(\omega_0) \frac{\partial \varepsilon(\omega_0)}{\partial \omega} \mathcal{H}_z^* \frac{\partial \mathcal{E}_x}{\partial t} + \text{c.c.} \right) + \dots \left. \right\}.\end{aligned}\quad (12)$$

We have simplified the notation by dropping the spatial dependence in both  $\varepsilon$  and  $\mu$ , and it is implied in what follows. In contrast, the Abraham momentum density is, more simply,

$$\begin{aligned}\mathbf{g}_{Abraham} &= \frac{\mathbf{E} \times \mathbf{H}}{4\pi c} \\ &= \frac{1}{4\pi c} \hat{\mathbf{z}} (\mathcal{E}_x \mathcal{H}_y^* + \mathcal{E}_x^* \mathcal{H}_y) - \frac{1}{4\pi c} \hat{\mathbf{y}} (\mathcal{E}_x \mathcal{H}_z^* + \mathcal{E}_x^* \mathcal{H}_z).\end{aligned}\quad (13)$$

For relatively slowly varying dielectric functions, the terms

shown in Eq. (12) are usually more than sufficient to accurately describe the dynamics, even for very short pulses (a few wave cycles in duration), because typical dispersion lengths may be on the order of meters, as we will see below. The expression for the force density function, Eq. (1), in the absence of free charges and free currents, may be written as

$$\begin{aligned} \mathbf{f}(\mathbf{r}, t) &= \rho_{\text{bound}} \mathbf{E} + \frac{1}{c} \left( \frac{\partial \mathbf{P}}{\partial t} + c(\nabla \times \mathbf{M}) \right) \times \mathbf{B} \\ &= \frac{1}{4\pi} \mathbf{E}(\nabla \cdot \mathbf{E}) + \frac{1}{4\pi c} \left[ \left( \frac{\partial \mathbf{D}}{\partial t} - \frac{\partial \mathbf{E}}{\partial t} \right) \right. \\ &\quad \left. + c \nabla \times \mathbf{B} - c \nabla \times \mathbf{H} \right] \times \mathbf{B}. \end{aligned} \quad (14)$$

We have made use of the usual constitutive relationships between the fields, namely  $\mathbf{D} = \mathbf{E} + 4\pi\mathbf{P}$  and  $\mathbf{B} = \mathbf{H} + 4\pi\mathbf{M}$ . Equation (14) includes a Coulomb contribution from bound charges, and contributions from bound dielectric polarization and magnetic current densities, in order to allow application to magnetically active materials. The Coulomb term shown may be expressed in a variety of ways. For example, using the first of Eqs. (11), and by using the condition  $\nabla \cdot \mathbf{D} = 0$ , one can show that, in the absence of absorption ( $\varepsilon \approx \varepsilon^*$ ), the Coulomb term takes the form

$$\begin{aligned} \frac{1}{4\pi\varepsilon} \left[ -\mathbf{E}(\nabla \cdot \varepsilon \cdot \mathbf{E}) + \omega_0 \mathbf{E} \left( \nabla \left. \frac{\partial \varepsilon}{\partial \omega} \right|_{\omega_0} \cdot \mathbf{E} \right) + \dots \right] \\ \times \left( 1 + \frac{1}{\varepsilon} \left. \frac{\partial \varepsilon}{\partial \omega} \right|_{\omega_0} + \dots \right). \end{aligned}$$

The presence of higher order terms is implied. The form given in Eq. (14) thus suggests that there is a Coulomb contribution if (i) the incident field has a TM-polarized component; (ii) scattering generally occurs from a three-dimensional structure with complex topology that generates other field polarizations; and (iii) if the field has curvature in all three dimensions. Under some circumstances, one may ignore the Coulomb contribution, for example by considering TE modes using our Eqs. (8), which lead directly to  $\nabla \cdot \mathbf{E} = \partial \mathcal{E}_x(y, z, t) / \partial x \equiv 0$ . This is a sufficient condition that may be easily satisfied in problems that exploit one- or two-dimensional symmetries, as we do here. It should be apparent, however, that more complicated topologies and/or the consideration of TM-polarized incident fields are in need of the general approach afforded by Eq. (14). In light of the previous discussion, we will first examine the case of TE-polarized incident pulses, and in the last section of the manuscript we will briefly discuss results that concern a TM-polarized pulse that traverses a single, ordinary dielectric interface. Therefore, for TE-polarized waves, Eq. (14) reduces to

$$\mathbf{f}(\mathbf{r}, t) = \frac{1}{4\pi c} \left( c \nabla \times \mathbf{B} - \frac{\partial \mathbf{E}(\mathbf{r}, t)}{\partial t} \right) \times \mathbf{B}. \quad (15)$$

Using Maxwell's equations, the total force can then be calculated as

$$\begin{aligned} \mathbf{F}(t) &= \int_{\text{volume}} d\mathbf{r}^3 \mathbf{f}(\mathbf{r}, t) \\ &= \int_{\text{volume}} \left[ \frac{1}{4\pi} \left( \mu \frac{\partial \mathbf{D}(\mathbf{r}, t)}{\partial t} - \frac{\partial \mathbf{E}(\mathbf{r}, t)}{\partial t} \right) \times \mathbf{B} \right] d\mathbf{r}^3 \\ &\quad + \frac{1}{4\pi} \int_{\text{volume}} \{ [(\nabla \mu) \times \mathbf{H}] \times \mathbf{B} \} d\mathbf{r}^3. \end{aligned} \quad (16)$$

In deriving Eq. (16) from Eq. (15), we have assumed that the magnetic permeability is approximately real and constant to show the basic contributions, including a surface term when the magnetic permeability is discontinuous. We will generalize this expression later when we deal with negative index materials.

Next, substituting Eqs. (8) and (11) into Maxwell's equations yields the following coupled differential equations [21–23]:

$$\begin{aligned} \alpha \frac{\partial \mathcal{E}_x}{\partial \tau} + i \frac{\alpha'}{4\pi} \frac{\partial^2 \mathcal{E}_x}{\partial \tau^2} - \frac{\alpha''}{24\pi^2} \frac{\partial^3 \mathcal{E}_x}{\partial \tau^3} + \dots \\ = i\beta [\varepsilon(\xi) \mathcal{E}_x - \mathcal{H}_z \sin \theta_i - \mathcal{H}_y \cos \theta_i] + \frac{\partial \mathcal{H}_z}{\partial \bar{y}} + \frac{\partial \mathcal{H}_y}{\partial \xi}, \\ \gamma \frac{\partial \mathcal{H}_y}{\partial \tau} + i \frac{\gamma'}{4\pi} \frac{\partial^2 \mathcal{H}_y}{\partial \tau^2} - \frac{\gamma''}{24\pi^2} \frac{\partial^3 \mathcal{H}_y}{\partial \tau^3} + \dots \\ = i\beta [\mu(\xi) \mathcal{H}_y - \mathcal{E}_x \cos \theta_i] - \frac{\partial \mathcal{E}_x}{\partial \xi}, \\ \gamma \frac{\partial \mathcal{H}_z}{\partial \tau} + i \frac{\gamma'}{4\pi} \frac{\partial^2 \mathcal{H}_z}{\partial \tau^2} - \frac{\gamma''}{24\pi^2} \frac{\partial^3 \mathcal{H}_z}{\partial \tau^3} + \dots \\ = i\beta [\mu(\xi) \mathcal{H}_z - \mathcal{E}_x \sin \theta_i] + \frac{\partial \mathcal{E}_x}{\partial \bar{y}}. \end{aligned} \quad (17)$$

Here

$$\begin{aligned} \alpha &= \left. \frac{\partial [\tilde{\omega} \varepsilon(\xi)]}{\partial \tilde{\omega}} \right|_{\omega_0}, & \alpha' &= \left. \frac{\partial^2 [\tilde{\omega} \varepsilon(\xi)]}{\partial \tilde{\omega}^2} \right|_{\omega_0}, \\ \gamma &= \left. \frac{\partial [\tilde{\omega} \mu(\xi)]}{\partial \tilde{\omega}} \right|_{\omega_0}, & \gamma' &= \left. \frac{\partial^2 [\tilde{\omega} \mu(\xi)]}{\partial \tilde{\omega}^2} \right|_{\omega_0}, \end{aligned}$$

and the prime symbol denotes differentiation with respect to frequency.  $\theta_i$  is the angle of incidence. The following scaling has been adopted:  $\xi = z/\lambda_r$ ,  $\bar{y} = y/\lambda_r$ ,  $\tau = ct/\lambda_r$ ,  $\beta = 2\pi\tilde{\omega}$ , and  $\tilde{\omega} = \omega/\omega_r$ , where  $\lambda_r = 1 \mu\text{m}$  is conveniently chosen as the reference wavelength. We note that nonlinear effects may be taken into account by adding a nonlinear polarization to the right-hand sides of Eqs. (17), as shown in Ref. [23], for example.

As we pointed out after the constitutive relation Eq. (9), the development that culminates with Eqs. (17) assumes that the medium is isotropic, a restriction that can be removed should the need arise, without impacting the relative simplicity of the approach or method of solution. Beyond this fact, Eqs. (17) do not contain any other approximations, but they

may be simplified depending on the circumstances. For example, in ordinary dielectric materials we may neglect second and higher order material dispersion terms, which eliminates second and higher order temporal derivatives. As an example, in the spectral region of interest, which includes the near IR range ( $\sim 800\text{--}1200\text{ nm}$ ), the dielectric function (actual data) of  $\text{Si}_3\text{N}_4$  [24] may be written as

$$\epsilon(\bar{\omega}) = 3.7798 + 0.178\,98\bar{\omega} + \frac{0.044\,08}{\bar{\omega}}. \quad (18)$$

Using this approximately linear dielectric susceptibility model, indeed we have  $\alpha'' = \{\partial^3[\bar{\omega}\epsilon(\xi)]/\partial\bar{\omega}^3\}|_{\omega_0} = 0$ . One may then estimate the second-order dispersion length, defined as  $L_D^{(2)} \sim \tau_p^2/|k''(\bar{\omega})|$ , where  $\tau_p$  is incident pulse width, and  $k''(\bar{\omega}) = \partial^2 k/\partial\bar{\omega}^2$ . The result is  $L_D^{(2)} \sim 2 \times 10^3 \lambda_r$  (or  $\sim 2\text{ mm}$ ) for an incident, five wave-cycle pulse ( $\sim 15\text{ fs}$ ); approximately 8 mm for a ten wave-cycle pulse; and 1 m for 100-wave cycle ( $\sim 300\text{ fs}$ ) pulses. In comparison, typical multilayer stacks and substrates that we consider range from a few microns to a few tens of microns in thickness, and so neglect of the second-order time derivative and beyond is completely justified, even for pulses only a few wave cycles in duration.

In the frequency range and the materials that we are considering, assuming for the moment that  $\mu = \gamma = 1$ , in our scaled coordinate system the simplified version of Eq. (12) is

$$\begin{aligned} \mathbf{g}_{\text{Minkowski}} = & \frac{\mathbf{D} \times \mathbf{B}}{4\pi c} = \frac{1}{4\pi c} \hat{\mathbf{z}} \left[ (\epsilon \mathcal{E}_x \mathcal{H}_y^* + \text{c.c.}) \right. \\ & \left. + \left( i \frac{1}{2\pi} \frac{\partial \epsilon}{\partial \bar{\omega}} \mathcal{H}_y^* \frac{\partial \mathcal{E}_x}{\partial \tau} + \text{c.c.} \right) + \dots \right] \\ & - \frac{1}{4\pi c} \hat{\mathbf{y}} \left[ (\epsilon \mathcal{E}_x \mathcal{H}_z^* + \text{c.c.}) \right. \\ & \left. + \left( i \frac{1}{2\pi} \frac{\partial \epsilon}{\partial \bar{\omega}} \mathcal{H}_z^* \frac{\partial \mathcal{E}_x}{\partial \tau} + \text{c.c.} \right) + \dots \right]. \quad (19) \end{aligned}$$

For nonmagnetic materials, Eq. (15) also simplifies to

$$\begin{aligned} \mathbf{f}(\mathbf{r}, t) = & \frac{1}{c} \frac{\partial \mathbf{P}(\mathbf{r}, t)}{\partial t} \times \mathbf{B}(\mathbf{r}, t) \\ = & \frac{1}{4\pi\lambda_r} \hat{\mathbf{z}} \left\{ i\beta(\epsilon^* - 1) \mathcal{E}_x^* \mathcal{H}_y - i\beta(\epsilon - 1) \mathcal{E}_x \mathcal{H}_y^* \right. \\ & \left. + \left[ (\alpha - 1) \frac{\partial \mathcal{E}_x}{\partial \tau} \mathcal{H}_y^* + (\alpha^* - 1) \frac{\partial \mathcal{E}_x^*}{\partial \tau} \mathcal{H}_y \right] + \dots \right\} \\ = & \frac{1}{4\pi\lambda_r} \hat{\mathbf{y}} \left\{ i\beta(\epsilon^* - 1) \mathcal{E}_x^* \mathcal{H}_z - i\beta(\epsilon - 1) \mathcal{E}_x \mathcal{H}_z^* \right. \\ & \left. + \left[ (\alpha - 1) \frac{\partial \mathcal{E}_x}{\partial \tau} \mathcal{H}_z^* + (\alpha^* - 1) \frac{\partial \mathcal{E}_x^*}{\partial \tau} \mathcal{H}_z \right] + \dots \right\}. \quad (20) \end{aligned}$$

Having defined the relevant momentum densities in Eqs. (12) and (13) above, the total momentum can then be easily calculated. In general one has two components, one longitudinal and one transverse, as follows [11]:

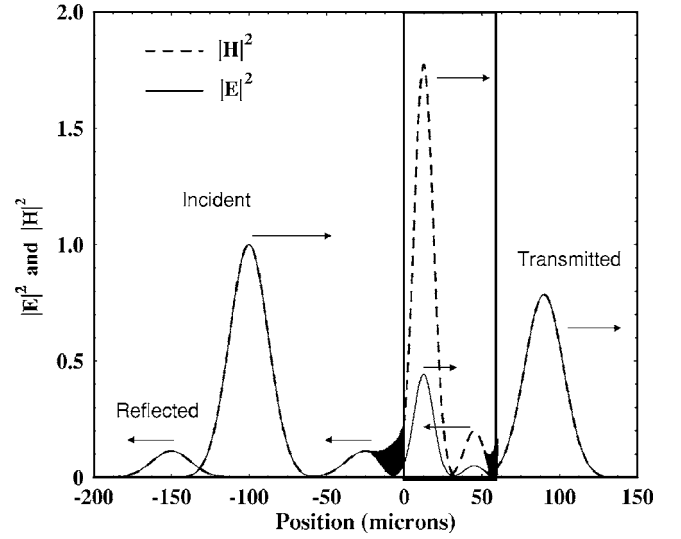


FIG. 1. A 100 fs pulse interacts with a  $60\ \mu\text{m}$  thick  $\text{Si}_3\text{N}_4$  substrate. Both E and H fields are shown as the pulse is partly transmitted and partly reflected from both entry and exit interfaces. Outside the structure the fields overlap, while inside pulse compression due to group velocity reduction and conservation of energy causes the magnetic field to increase its amplitude with respect to the incident field.

$$\begin{aligned} P_\xi(\tau) = & \int_{\xi=-\infty}^{\xi=\infty} d\xi \int_{\tilde{y}=-\infty}^{\tilde{y}=\infty} g_\xi(\tilde{y}, \xi, \tau) d\tilde{y}, \\ P_{\tilde{y}}(\tau) = & \int_{\xi=-\infty}^{\xi=\infty} d\xi \int_{\tilde{y}=-\infty}^{\tilde{y}=\infty} g_{\tilde{y}}(\tilde{y}, \xi, \tau) d\tilde{y}. \quad (21) \end{aligned}$$

These components may be used to calculate the angle of refraction [21]. To simplify matters further, for the moment we assume that the pulse is incident normal to the multilayer surface, i.e.,  $P_{\tilde{y}}(\tau) = 0$  at all times, and focus our attention on the longitudinal component. Finally, assuming no frictional or other dissipative forces are present, conservation of momentum requires that the linear momentum imparted to the structure be given by

$$P_{\text{structure}}(\tau) = P_\xi^0 - P_\xi(\tau), \quad (22)$$

where  $P_\xi^0 = P_\xi(\tau=0) = \int_{\xi=-\infty}^{\xi=\infty} d\xi \int_{\tilde{y}=-\infty}^{\tilde{y}=\infty} g_\xi(\tilde{y}, \xi, \tau=0) d\tilde{y}$  is the total momentum initially carried by the pulse in free space, before it enters any medium. The force may then be calculated as the temporal derivative of the momentum in Eq. (22).

### A thick, uniform substrate

In this section we consider the interaction of a  $1\text{ MW/cm}^2$  Gaussian pulse of the type  $\mathcal{E}_x(\tilde{y}, \xi, \tau=0) = E_0 e^{-[(\xi-\xi_0)^2 + \tilde{y}^2]/w^2}$ , and similarly for the transverse magnetic field, with a  $60\ \mu\text{m}$  thick  $\text{Si}_3\text{N}_4$  substrate, as depicted in Fig. 1. Choosing  $w \sim 20$  corresponds to a  $1/e$  width of approximately 100 fs in duration, but we note that the exact temporal duration of the pulse is not crucial. The spatial extension (both longitudinal and transverse) of the pulse in free space may be estimated from the figure at about  $40\ \mu\text{m}$

( $1/e$  width). Inside the medium, the longitudinal spatial width is compressed by roughly a factor proportional to the group index, and from the figure it is clear that at some point the pulse is completely embedded inside the medium, so that a steady-state dynamics is reached after the entire pulse crosses the entry surface. Once the pulse reaches the exit interface, most of it is transmitted as part of it reflects back toward the entry interface, so that the energy leaks out relatively slowly from both sides of the substrate. We now describe some basic facts intrinsic to the event.

The index of refraction of the substrate at the carrier wavelength ( $\lambda_0=1 \mu\text{m}$ ) is  $n \sim 2$ . The transmittance through the surface may be computed as the fraction of energy transmitted with respect to the incident energy. When dispersion is present, the electromagnetic energy density may be generalized as follows [22]:

$$U(\vec{y}, \xi, \tau) = \alpha_r |\mathcal{E}_x|^2 + \beta_r |\mathcal{H}_y|^2 + \frac{i\alpha_r'}{4\pi} \left( \mathcal{E}_x^* \frac{\partial \mathcal{E}_x}{\partial \tau} - \mathcal{E}_x \frac{\partial \mathcal{E}_x^*}{\partial \tau} \right) + \frac{i\beta_r'}{4\pi} \left( \mathcal{H}_y^* \frac{\partial \mathcal{H}_y}{\partial \tau} - \mathcal{H}_y \frac{\partial \mathcal{H}_y^*}{\partial \tau} \right) + \dots, \quad (23)$$

where  $\alpha_r = \text{Re}(\alpha)$ ,  $\beta_r = \text{Re}(\beta)$ , and the symbol  $'$  once again means differentiation with respect to the frequency. The total energy can be calculated by integrating Eq. (23) over all space, namely  $W_T(\tau) = \int_{-\infty}^{\infty} d\vec{y} \int_{-\infty}^{\infty} d\xi U(\vec{y}, \xi, \tau)$ . Our calculations yield a transmittance consistent with the usual transmittance function:  $T=4n/(n+1)^2$  ( $T=0.888$  for  $n=2$ ). Evaluation of the linear momentum yields a momentum transfer through the first interface that is identical to the result of Eq. (2) obtained in the quantum regime [15], with the proper positive sign. For example, for  $n=2$  Eq. (2) predicts that  $2/3$  of the initial momentum is transferred to the substrate, and that is precisely what we find (see Fig. 2). However, when it comes to the exit interface, the results differ somewhat from those quoted in Ref. [15], but are qualitatively similar. In any case, our calculated, final slab momentum is  $P_{final} \approx 0.38P_0$ . To illustrate this, in Fig. 2 we plot the total linear momentum gained by the substrate as a function of time at the expense of the fields, normalized with respect to the total initial momentum carried by the pulse, as calculated using Eqs. (12), (13), and (22). Here we see that the Abraham momentum is always positive, while the Minkowski momentum becomes negative during the first interface crossing. This implies that to conserve momentum the substrate should move toward the pulse or equivalently, be attracted by it. Therefore, the Abraham and Minkowski momenta predict that the substrate will move in opposite directions. However, the figure also shows that when the pulse exits to the right of the substrate, the total Minkowski momentum reacquires a positive value not too dissimilar from the Abraham momentum, as now most of the pulse is located in free space. This small discrepancy is due to the fact that a small fraction of the pulse still lingers inside the substrate, as it reflects back and forth from the entry and exit interfaces.

In Fig. 3 we show the longitudinal Lorentz force calculated using our Eq. (20) (triangles) and compare it to the time derivatives of the Abraham (solid line) and Minkowski mo-

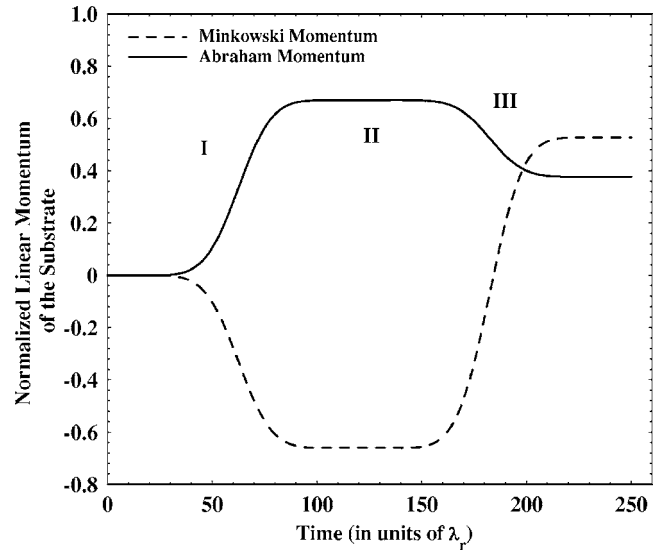


FIG. 2. Linear momentum transferred to the substrate using the Minkowski (dashed) and Abraham (solid) momenta, normalized with respect to the total incident momentum. The Minkowski momentum predicts that the momentum transferred to the structure will be negative during and after the first interface crossing. The slab gains a linear momentum of  $\sim 2/3$  of the initial momentum upon crossing the first interface. The final momentum of the slab, after most of the energy has leaked out, is close to 38% of the initial momentum.

menta (dashed). The figure clearly shows that the Abraham and Lorentz forces overlap during the entire process, while the Minkowski momentum never represents the Lorentz force to any degree, except in the trivial case of zero force. In

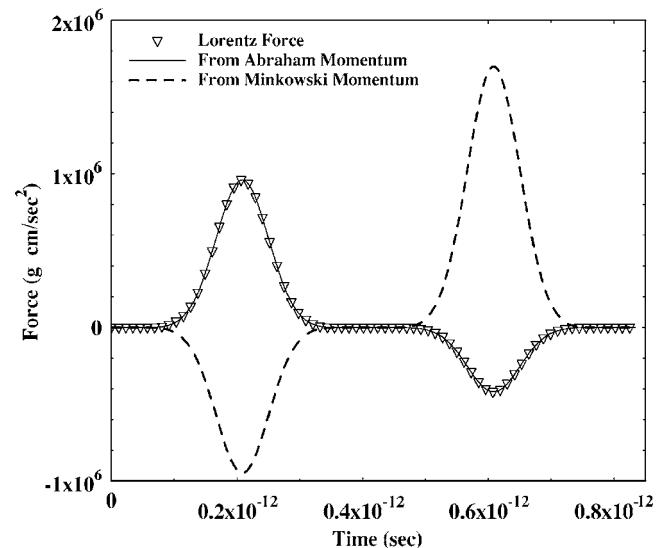


FIG. 3. Lorentz force calculated using Eq. (20) (open triangles), force calculated using the Abraham (solid) and Minkowski (dashed) momenta. It is evident that only the Abraham momentum leads to the Lorentz force and tracks it almost exactly during the entire time. The Abraham force is always directed toward the substrate, as indicated by the sign change of the force, upon entry and upon exit from the substrate, and the Minkowski force has always the opposite sign.

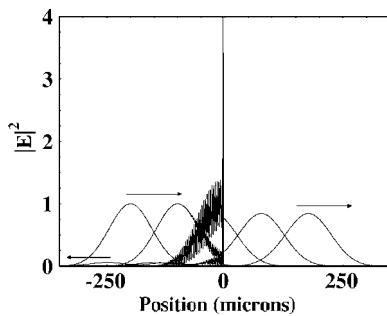


FIG. 4. Scattering of a 600 fs incident pulse from a  $4 \mu\text{m}$  multilayer structure composed of 15 periods of  $\text{Si}_3\text{N}_4(125 \text{ nm})/\text{SiO}_2(150 \text{ nm})$ , having a mass  $m \sim 10^{-5} \text{ g}$ , and volume  $V \approx 4 \times 10^{-12} \text{ m}^3$ . Most of the pulse is always located in free space during the entire interaction, a fact that eventually causes the Abraham and Minkowski momenta to be similar.

Ref. [15] the total momentum transferred to the structure is calculated by performing the time integral of the total calculated force. It is evident even from Fig. 3 that this procedure may, under the right circumstances, yield similar areas for both the Minkowski and Abraham momenta, especially if one waits for the pulse to leave the structure. However, calculation of the forces via direct integration of Maxwell's equation, accompanied by a direct evaluation of the Abraham and Minkowski momenta, reveals unmistakable agreement between the Abraham and the Lorentz forces. Based on this example, our conclusion is that it is generally not possible for the Minkowski momentum, the averaged momentum Eq. (3), or any other plausible definition of momentum that uses the fields, to accomplish the same thing in substrates or other similar extended media.

### III. PHOTONIC BAND GAP STRUCTURES

We now consider a typical finite multilayer sample. We assume the stack is composed of 15 periods of generic, representative, dispersive materials with dielectric constants  $\epsilon_1 \approx 2$  (as in  $\text{SiO}_2$ ) and  $\epsilon_2 \approx 4$  [as in  $\text{Si}_3\text{N}_4$ , and we use the dispersion function of Eq. (18) above] over the entire near IR range. Assuming a cross section of approximately  $1 \text{ mm}^2$  and a thickness of  $\sim 4 \text{ microns}$  ( $\text{SiO}_2$  layers are taken to be 150 nm thick, and that  $\text{Si}_3\text{N}_4$  layers are 125 nm thick), the volume of the structure is  $V \approx 4 \times 10^{-12} \text{ m}^3$ . Using the known material densities of  $\text{SiO}_2$  and  $\text{Si}_3\text{N}_4$ , the mass of the structure can be estimated at  $m \sim 10^{-5} \text{ g}$ . For the moment we neglect the presence of a substrate, and assume the beam waist is at least several tens of wave cycles wide, so that we may also neglect diffraction effects.

In Fig. 4 we show a typical scattering event when the carrier frequency of a narrow-band pulse [4] is tuned at the first resonance near the band edge. The structure is located near the origin, and with a spatial extension of only 4 microns, it is evident that most of the pulse is located outside the structure most of the time: this is the primary reason why the Minkowski and Abraham momentum densities generally differ little during the interaction. In Fig. 5 we show the electric and magnetic field profiles inside the

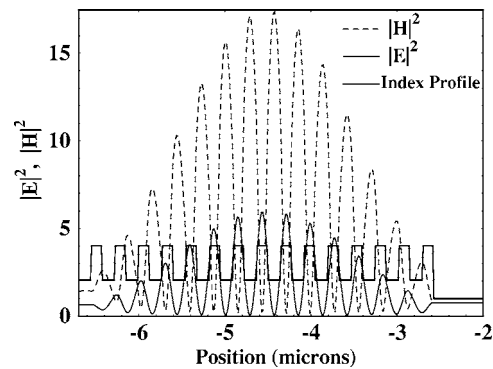


FIG. 5. Electric and magnetic field localization properties of a light pulse tuned at the photonic band edge. The electric and magnetic fields are spatially delocalized, resulting in small group and energy velocities. The y-axis scaling reflects the magnitude of the fields inside the structure relative to the input intensity. This kind of field localization and enhancement, which carries momentum and energy, is not available for simple Fabry-Perot etalons.

multilayer stack. The fields are delocalized with minimum overlap, leading to small group and energy velocities [4]. Because the transverse field profiles do not change, we resort to plotting just the longitudinal, axial cross section of the pulse.

In Fig. 6 we compare the Minkowski and Abraham momenta calculated using Eqs. (12) and (13) for a pulse approximately 100 fs in duration for two different conditions: tuning at the band edge resonance, and inside the gap. The calculations show that when the carrier wavelength is tuned inside the gap, so that the structure acts like a mirror (the transmittance is less than  $10^{-3}$ ), there is effectively no difference between the two momenta, and so the curves overlap

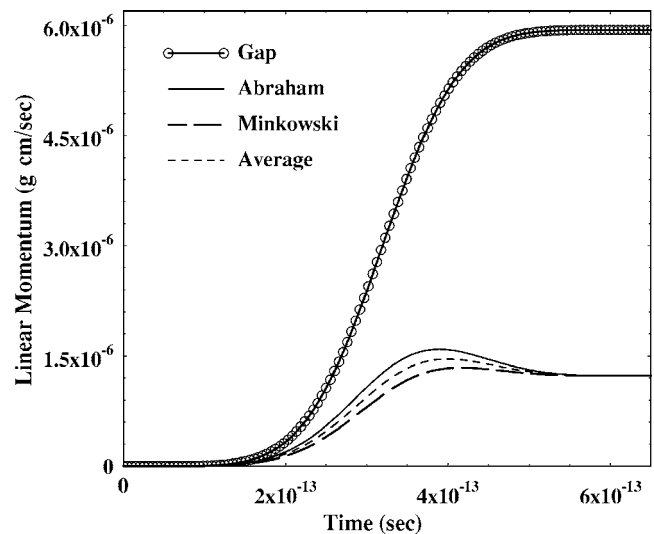


FIG. 6. Abraham and Minkowski momenta for a 100 fs pulse tuned inside the gap (solid line overlapped by open circles) and for the same pulse tuned at the band edge resonance (thin solid and long dashes). The average momentum is also calculated (thin dashes). The Abraham and Minkowski momenta yield similar results because in both cases the pulse is located mostly in free space during the entire time, as the structure is only a few microns thick.

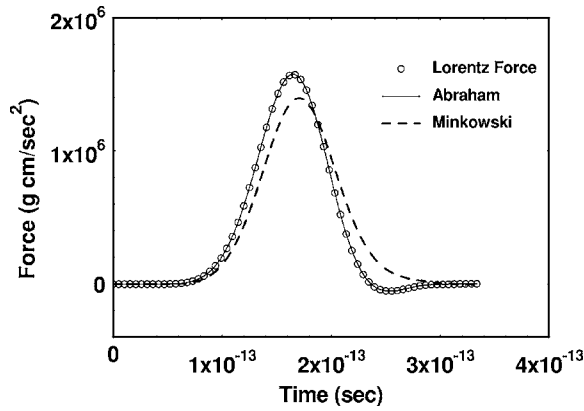


FIG. 7. Lorentz force (open triangles), Abraham force (solid curve), and Minkowski (dashed) force obtained from the time derivative of the respective momenta, depicted in Fig. 6. Small differences notwithstanding, the Abraham force tracks the Lorentz force to better than one part in a thousand. However, the total integrated areas under the Abraham and Minkowski curves, which represent the total momentum transferred, have the same value to at least one part in one thousand.

(solid line with open circles). The pulse remains mostly outside the structure, as the penetration depth (or skin depth) amounts to only a small fraction of a wavelength.

Tuning the pulse at resonance results in field localizations similar to those of Fig. 5 and leads to slightly different and distinguishable curves. However, it is also clear that any differences are transient, as only a tiny portion of the pulse occupies the structure at any given time. For all intents and purposes either representation may be used to obtain the order of magnitude of the total momentum transferred. Nevertheless, taking the time derivatives of the momenta shown in Fig. 6, for the pulse tuned at the band edge, results in the total force experienced by the structure, which we show in Fig. 7. The figure clearly shows that even though differences are small, it is only the Abraham momentum that once again coincides almost exactly with an independent calculation of the Lorentz force, Eq. (20), even though the integrated areas under the curves yield almost identical results, with differences in the range of one part in a thousand.

In Figs. 8 and 9 we show the predicted force and displacement, respectively, associated with a mass of  $10^{-5}$  g acted upon by a Gaussian pulse approximately 600 fs in duration, and peak power of  $1 \text{ MW/cm}^2$ , once again tuned at resonance. Although Fig. 8 suggests remarkably high accelerations, with maxima of  $\sim \pm 5 \times 10^{10} \text{ cm/s}^2$  (force/mass), Fig. 9 suggests that the magnitudes of the displacement and associated velocity [calculated using the simple classical expressions  $X(t) \approx x_0 + vt + \frac{1}{2}at^2$  and  $V(t) \approx at$ ] are tempered by the extremely short interaction times. We note that both Abraham and Minkowski momenta yield similar results, due to the finite extent of the structure.

Tuning at a band edge resonance produces a more peculiar and ostensibly more intriguing dynamics, as Figs. 6–9 suggest. While the pulse generally exerts a force always directed toward the structure upon entering and upon exiting the medium, using finite bandwidth pulses means that the structure will be left with some residual momentum, as finite

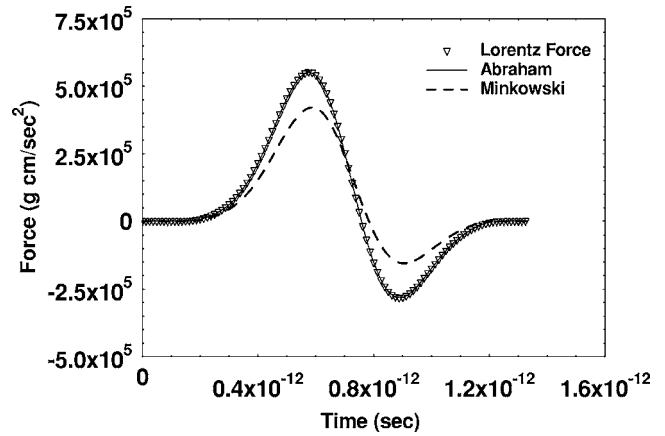


FIG. 8. Force versus time experienced by the free-standing multilayer stack, corresponding to an incident, 600 fs pulse tuned at resonance, just as in Fig. 6. The bandwidth of the present pulse is approximately six times narrower compared to that of Fig. 6, which leads to better field localization and smaller overall reflection. Tuning the carrier frequency of the pulse at resonance leads to negative forces, with correspondingly negative accelerations, just as in the case of Fig. 3. Depending on pulse duration and bandwidth, this oscillatory motion may be sustained by a well-timed train of incident pulses. Only the Abraham force is seen to accurately reproduce the Lorentz force.

amounts of energy and momentum are always reflected. For example, referring to Figs. 8 and 9, we find that the structure begins to move forward as energy and momentum are stored inside it. In addition to field localization effects, tuning a relatively narrow-band pulse at resonance guarantees that it will reacquire *nearly* all of its initial forward momentum, within the bounds dictated by the bandwidth of the pulse. Therefore, we find that the pulse centroid always pushes in the direction of the structure, consistent with previous predictions [15,16], and as the peak of the pulse spills over to the right of the barrier the structure is pushed backward. This can be discerned by the fact that the instantaneous accelera-

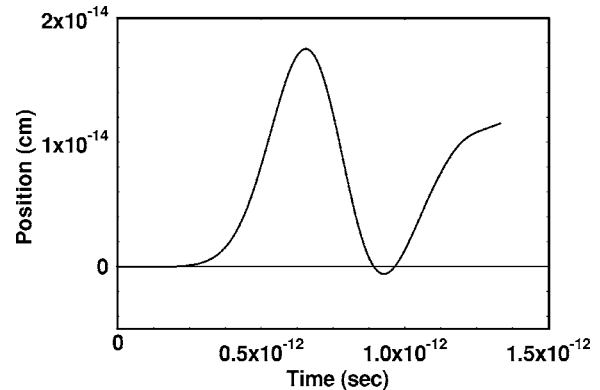


FIG. 9. Longitudinal displacement that corresponds to the Abraham force (and acceleration) shown in Fig. 8. The structure is pushed forward, returns to the origin, but eventually acquires forward terminal velocity. The cavity stores energy and momentum, with a relatively long tail that may keep the structure moving back and forth, depending on pulse bandwidth and tuning with respect to the band edge.

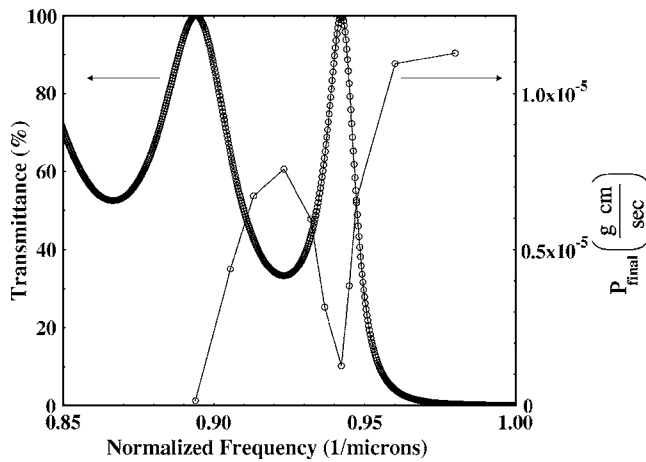


FIG. 10. Plane-wave transmittance (left y axis) and total momentum transferred (right y axis) for the structure described in Fig. 4. A changing transmittance and field localization properties near the band edge lead to widely tunable total momentum transfer.

tion changes sign (Fig. 8). Furthermore, forward motion is almost compensated by its backward movement, and the structure tends to return to its original position (Fig. 9). However, the device is literally immersed inside fields that will continue to push and pull as long as light lingers inside the cavity. In general, the structure may oscillate about the origin, or move forward, begin to turn back, and then move forward again. In this case the oscillation is ultimately followed by a forward terminal velocity. These dynamics, and the ultimate direction of motion of a free-standing mass, for the most part depend on the tuning condition with respect to the band edge, and the bandwidth of the incident pulse. This particular example clearly does not exhaust the possibilities.

Finally, in Fig. 10 we plot the plane-wave transmittance of the structure (left y axis), calculated using the matrix transfer technique. On the right y axis we plot the total linear momentum gained by the multilayer stack versus normalized frequency, as calculated using the Abraham momentum [Eq. (13)]. In this instance we again use 600 fs incident pulses to better resolve the resonances. The figure clearly suggests that the amount of momentum transferred to the structure is widely tunable because of the diverse field localization properties that occur near the band edge, with minimum but non-zero momentum transfer at resonance, and mirrorlike reflections and maximum momentum transfer when the pulse is tuned inside the gap.

The total momentum transferred, and hence displacements, may be increased in at least three ways: (i) by increasing pulse duration, (ii) by sending a train of pulses, or (iii) by increasing pulse peak power. For example, a group of  $10^6$  pulses pushes the overall displacement in the nanometer range. If we increase pulse duration to 100 ps, then the structure's displacement becomes of the same order of magnitude required to observe interference effects due to radiation pressure in MEMS environments [10]. In general, the degree of sensitivity appears to be remarkably high, but it may be further increased by either decreasing the number of incident pulses or by reducing peak power. One may envision applications to ultra-high sensitive torsional balances and pressure gauges, for example.

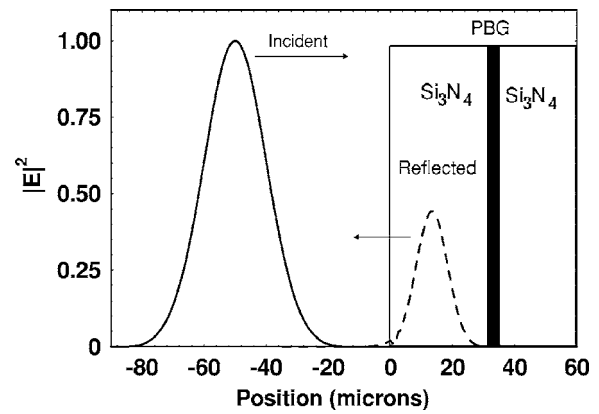


FIG. 11. The same structure described in the text and in the caption of Fig. 4 is now embedded inside a background dielectric medium, chosen here to be  $\text{Si}_3\text{N}_4$ . The figure shows both the incident pulse and the pulse reflected from the embedded mirror while it is still located inside the entry substrate. Transmittance through the Bragg mirror is less than  $10^{-3}$ .

We now examine the case of a photonic band gap structure immersed inside a background dielectric material whose index of refraction is other than unity. In the example we place the same multilayer stack that we used in the previous section in the middle of a dielectric substrate, akin to a reflective membrane immersed in a liquid, and tune the carrier frequency of the incident pulse inside the photonic band gap to utilize the structure as a mirror. The advantage of this situation with respect to an ordinary metallic mirror is that we have no material absorption to consider or interpret, thus leaving no doubt as to how the energy and momentum are utilized. The situation is depicted in Fig. 11, where we show the incident and reflected pulses, and the multilayer stack immersed inside a  $\text{Si}_3\text{N}_4$ -like background medium. The entry substrate is thick enough to contain the entire pulse, so that a steady-state dynamics is reached. In Fig. 12 we show the predicted momenta. The time evolution of the momentum tracks the pulse as it crosses the entry interface (I), impacts the mirror (II), and turns back toward the entry surface (III). We stop the pulse while it remains inside the substrate, because discrepancies between the momenta are largest there.

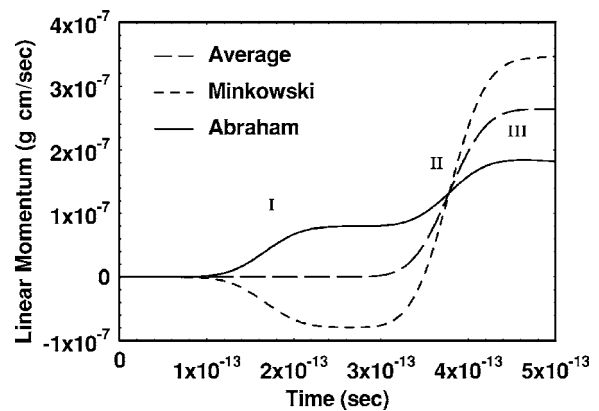


FIG. 12. Abraham (solid curve), Minkowski (short dashes), and average (long dashes) momenta for the case depicted in Fig. 11.

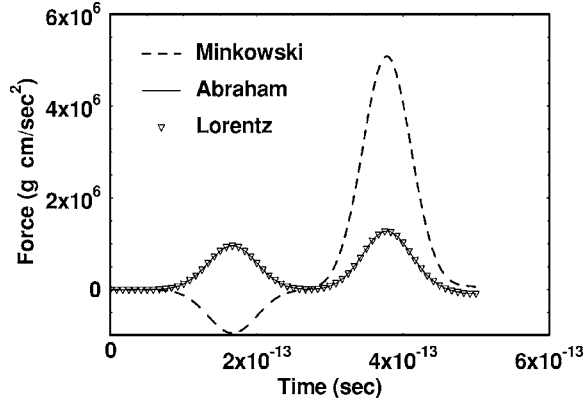


FIG. 13. The forces at play in the situation described in Figs. 11 and 12. Only the Abraham force once again tracks the Lorentz force very well during the entire time.

In fact, the figure shows that the Abraham and Minkowski momenta may differ by as much as a factor of 2, as long as the pulse is still located inside the substrate. The two momenta converge to roughly the same value if the pulse is allowed to exit back into free space. The plateau between regions I and II represents the pulse in transit toward the mirror. Therefore, any detection scheme designed to discern any significant differences should detect motion of the reflective membrane before the pulse exits back into vacuum. Just as we did before, we now determine the Lorentz force, Eq. (20), from the fields that result from the integration of Max-

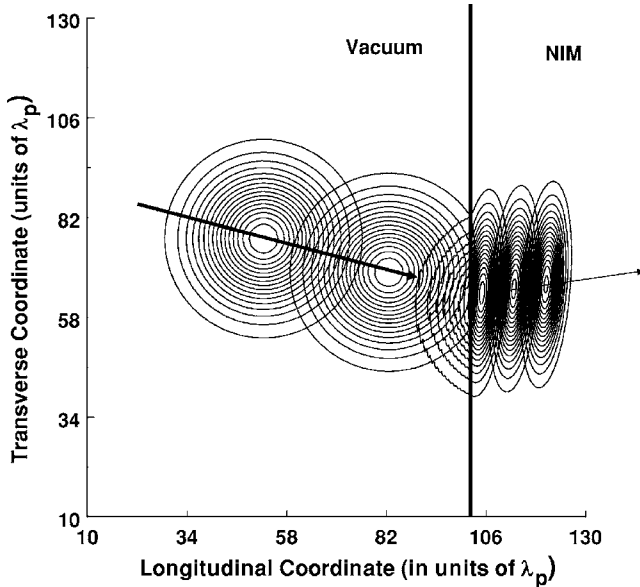


FIG. 14. A pulse approximately 30 wave cycles wide (thus 30 wave cycles in duration) crosses an interface that separates vacuum from a negative index material at an angle of  $15^\circ$ . We note that in the Drude model, causality's only demand is that  $\gamma \neq 0$ . These conditions cause the pulse to refract anomalously in the upper quadrant, while the pulse distorts in both real and Fourier space. The result is a wave packet whose Poynting vector points forward in the direction of propagation, and a wave vector that points backwards, toward the entry surface [21]. We stop the pulse while it is still located inside the substrate.

well's equations (17), compare with the temporal derivatives of the Abraham and Minkowski momenta, and plot the results in Fig. 13. The figure comments itself, as once again the Lorentz force is closely tracked only by the Abraham force.

#### IV. NEGATIVE INDEX MATERIALS

In negative index materials, the Lorentz force density is slightly more complex because all the terms in Eq. (16) contribute. The resulting generalized expression for the longitudinal and transverse components of the Lorentz force density, assuming both  $\epsilon$  and  $\mu$  are complex, may be written as follows:

$$\begin{aligned} \mathbf{f}(\mathbf{r}, t) = & \frac{1}{4\pi\lambda_r} \hat{\mathbf{z}} \left[ i\beta[\mu(\mu^* \epsilon^* - 1)\mathcal{E}_x^* \mathcal{H}_y - \mu^*(\mu\epsilon - 1)\mathcal{E}_x \mathcal{H}_y^*] \right. \\ & + \mu(\alpha^* \mu^* - 1)\mathcal{H}_y \frac{\partial \mathcal{E}_x^*}{\partial \tau} + \mu^*(\mu\alpha - 1)\mathcal{H}_y^* \frac{\partial \mathcal{E}_x}{\partial \tau} \\ & \left. - \left( \frac{\partial |\mu|^2}{\partial \xi} \right) |\mathcal{H}_y|^2 + \dots \right] \\ & - \frac{1}{4\pi\lambda_r} \hat{\mathbf{y}} \left[ i\beta[\mu(\mu^* \epsilon^* - 1)\mathcal{E}_x^* \mathcal{H}_\xi \right. \\ & - \mu^*(\mu\epsilon - 1)\mathcal{E}_x \mathcal{H}_\xi^*] + \mu(\alpha^* \mu^* - 1)\mathcal{H}_\xi \frac{\partial \mathcal{E}_x^*}{\partial \tau} \\ & + \mu^*(\mu\alpha - 1)\mathcal{H}_\xi^* \frac{\partial \mathcal{E}_x}{\partial \tau} \\ & \left. - \left( \mu \frac{\partial \mu^*}{\partial \xi} \mathcal{H}_y^* \mathcal{H}_\xi + \mu^* \frac{\partial \mu}{\partial \xi} \mathcal{H}_y \mathcal{H}_\xi^* \right) + \dots \right]. \quad (24) \end{aligned}$$

For simplicity, we have retained only the lowest order terms. A simple comparison reveals that Eq. (24) reduces to Eq. (20) when there are no magnetic contributions, as it should. Each part of Eq. (24) displays a magnetic component that contains the longitudinal spatial derivative of the magnetic permeability. If  $\mu$  is discontinuous, some care should be exercised when the volume integrals of Eq. (24) are evaluated. As before, the fields found in Eq. (24) are calculated using Maxwell's equations (17). Because typical dispersion lengths in negative index materials may easily exceed several hundred wavelengths [20–23], Eqs. (17) may once again be simplified by retaining terms up to and including the first-order temporal derivatives on both fields. The reference wavelength is now taken to be the plasma frequency, so that  $\lambda_r = \lambda_p$ . In our case and in our units, for incident 30 wave cycle pulses,  $L_D^{(2)} \approx \tau_p^2 / |k''(\bar{\omega})| = 30^2 / 1.6 = 562\lambda_p$ , which justifies our neglect of second and higher order temporal derivatives. In Fig. 14 we depict the typical dynamics that ensues as a result of integrating the system of equations (17) when the substrate is magnetically active; we use the Drude model to describe both  $\epsilon$  and  $\mu$  to enforce a causal response, and use:  $\epsilon(\bar{\omega}) = \mu(\bar{\omega}) = 1 - 1/(\bar{\omega}^2 + i\bar{\omega}\gamma)$ .

The pulse is incident at a  $15^\circ$  angle, and its carrier frequency is tuned at  $\omega = 0.577$ , where both  $\epsilon(\bar{\omega}) = \mu(\bar{\omega}) \approx -2$ , and  $\partial(\epsilon\bar{\omega})/\partial\bar{\omega} = \partial(\mu\bar{\omega})/\partial\bar{\omega} \sim 4$ . We choose  $\gamma = 10^{-5}$ , which

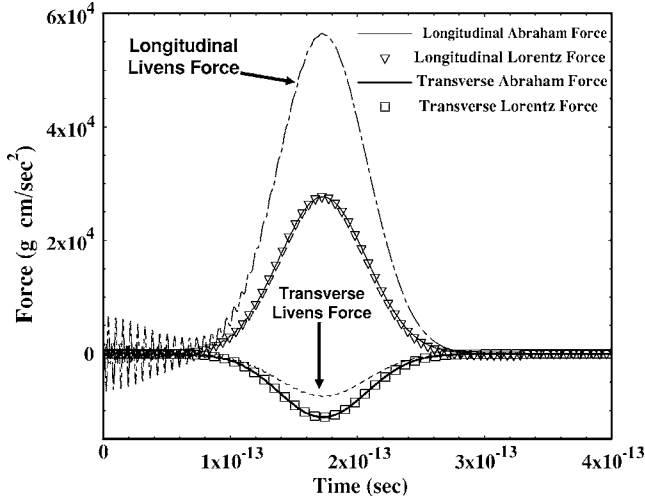


FIG. 15. Longitudinal (empty triangles) and transverse (open squares) Lorentz forces, compared to the same quantities computed from the Abraham momentum (solid thin curve: longitudinal; solid thick curve: transverse). The arrows point to both the longitudinal and transverse Livens forces. Once again, the agreement between the prediction of the Abraham momentum and the Lorentz force is obvious, and it remains unmatched by all competing definitions, including the Minkowski momentum (not shown in the figure).

yields no discernable absorption for relatively short propagation distances. Inside the substrate, the energy and group velocities are both positive and equal, with a value of approximately  $V_g = V_E \approx c/4$  [21]. The front of the transmitted wave packet distorts and refracts in a direction consistent with Snell's law, but with a negative index of refraction. The pulse initially contains both longitudinal and transverse momenta, as it is launched at an angle with respect to the surface. Because the conditions found in a NIM environment are much more stringent and unique compared to conditions existing in ordinary materials, it provides an ideal environment to test the conservation laws.

In magnetically active materials, one may also consider a competing definition of momentum density, namely  $\mathbf{g}_L = (\mathbf{E} \times \mathbf{B})/4\pi c$ , due to Livens [25], which in our case becomes

$$\mathbf{g}_L = \frac{\mathbf{E} \times \mathbf{B}}{4\pi c} = \frac{1}{4\pi c} \hat{\mathbf{z}} \left[ \mu^* \mathcal{E} \mathcal{H}_y^* + \mu \mathcal{E}^* \mathcal{H}_y + \frac{i}{2\pi} \left( \frac{\partial \mu}{\partial \omega} \mathcal{E}^* \frac{\partial \mathcal{H}_y}{\partial \tau} - \frac{\partial \mu^*}{\partial \omega} \mathcal{E} \frac{\partial \mathcal{H}_y^*}{\partial \tau} \right) + \dots \right] - \frac{1}{4\pi c} \hat{\mathbf{y}} \left[ \mu^* \mathcal{E} \mathcal{H}_z^* + \mu \mathcal{E}^* \mathcal{H}_z + \frac{i}{2\pi} \left( \frac{\partial \mu}{\partial \omega} \mathcal{E}^* \frac{\partial \mathcal{H}_z}{\partial \tau} - \frac{\partial \mu^*}{\partial \omega} \mathcal{E} \frac{\partial \mathcal{H}_z^*}{\partial \tau} \right) + \dots \right]. \quad (25)$$

In Fig. 15 we show the longitudinal and transverse Abraham and Livens forces and compare them with the volume integral of the Lorentz force, Eq. (24). We also calculate the Minkowski force, but for clarity we do not show it in the figure. Once again we find that it is only the Abraham momentum that accurately describes the conservation of linear momentum every step of the way, even under these extreme conditions. Therefore, one can reasonably conclude that any

other plausible definition of momentum density cannot provide a viable alternative, including the Livens and Minkowski momentum densities.

## V. TM POLARIZATION

We now briefly comment on the case of TM-polarized, incident pulses, which may be described as follows:

$$\mathbf{H} = \hat{\mathbf{x}}(\mathcal{H}_x(y, z, t)e^{i(k_z z - k_y y - \omega_0 t)} + \text{c.c.})$$

$$\mathbf{E} = \hat{\mathbf{y}}(\mathcal{E}_y(y, z, t)e^{i(k_z z - k_y y - \omega_0 t)} + \text{c.c.}) + \hat{\mathbf{z}}(\mathcal{E}_z(y, z, t)e^{i(k_z z - k_y y - \omega_0 t)} + \text{c.c.}). \quad (26)$$

For simplicity, we assume that a 30-wave cycle ( $\sim 1/e$  width) pulse is obliquely incident on a  $\text{Si}_3\text{N}_4$  substrate. We use this material because for relatively short propagation distances we can neglect absorption ( $\varepsilon \approx \varepsilon^*$ ) and assume weak dispersion ( $\alpha = \partial[\tilde{\omega}\varepsilon]/\partial\tilde{\omega}|_{\omega_0} \approx \varepsilon$ ). In this limit, the Coulomb term [i.e., the expression below Eq. (14)] reduces to  $(1/4\pi)\mathbf{E}(\nabla \cdot \mathbf{E}) = -(\mathbf{E} \cdot \nabla \varepsilon/4\pi\varepsilon)\mathbf{E}$ . The Lorentz force density Eq. (20) may then be written as follows:

$$\mathbf{f}(\mathbf{r}, t) \approx \frac{(\varepsilon - 1)}{4\pi\lambda_r} \hat{\mathbf{z}} \left[ i\beta(\mathcal{E}_y \mathcal{H}_x^* - \mathcal{E}_y^* \mathcal{H}_x) - \left( \mathcal{H}_x \frac{\partial \mathcal{E}_y^*}{\partial t} + \mathcal{H}_x^* \frac{\partial \mathcal{E}_y}{\partial t} - \frac{1}{4\pi\varepsilon} \frac{\partial \varepsilon}{\partial z} 2|\mathcal{E}_z|^2 + \dots \right) \right] - \frac{(\varepsilon - 1)}{4\pi\lambda_r} \hat{\mathbf{y}} \left[ i\beta(\mathcal{E}_z^* \mathcal{H}_x - \mathcal{E}_z \mathcal{H}_x^*) + \left( \mathcal{H}_x \frac{\partial \mathcal{E}_z^*}{\partial t} + \mathcal{H}_x^* \frac{\partial \mathcal{E}_z}{\partial t} \right) + \frac{1}{4\pi\varepsilon} \frac{\partial \varepsilon}{\partial z} (\mathcal{E}_x \mathcal{E}_y^* + \mathcal{E}_z^* \mathcal{E}_y) + \dots \right]. \quad (27)$$

Just as was the case for negative index materials, the volume integral of Eq. (27) contains surface terms that result from a longitudinal, dielectric discontinuity that cannot be ignored and, as before, care should be exercised in the evaluation of the surface integrals. Nevertheless, we once again find that only the Abraham momentum leads to an accurate description of the Lorentz force, as expected.

## VI. CONCLUSIONS

For almost a century the debate regarding the basic electromagnetic conservation laws in macroscopic media has continued unabated, and it will probably continue for some time to come. In this study we have used a numerical approach to solve the vector Maxwell's equation when dispersion is present, and established that, under a variety of circumstances, conditions, and media, the conservation of linear momentum may be understood solely in terms of the Poynting vector and Abraham momentum density. Gordon showed [18] that our Eq. (7) is in fact the relevant conservation law even in the presence of matter. The presence of magnetic activity must be taken into account with some caution, but given the guidance that our numerical evidence provides, it should be possible to generalize Gordon's expression for arbitrary  $\varepsilon$  and  $\mu$ .

In summary, we have treated the propagation of short pulses in ordinary materials in the form of extended substrates and periodic structures located in free space, as well as embedded inside a background material, such as a liquid. We have also studied the traversal of an interface that separates vacuum from a negative index material. The basic result that consistently emerges from this investigation is that in all cases we find that an independent evaluation of the Lorentz force is invariably consistent only with the Abraham momentum, leaving no doubt that the basic momentum conservation law should ultimately clearly reflect this fact. The results are found consistently in both one- and two-dimensional topologies, for both TE and TM polarized fields.

Because what is mechanical and what is electromagnetic remains mostly a matter of debate and interpretation of the

various terms that enter into the Lorentz force, our results should be viewed through the same lens, and stricter interpretations will ultimately have to be found within the results of new, more refined experimental evidence. Nevertheless, using well-established methods and techniques, and using a well-established starting point, i.e., an expression for the Lorentz force, the numerical evidence that we uncover points consistently to a simple fact: that the only electromagnetic momentum of consequence is the Abraham momentum.

#### ACKNOWLEDGMENT

G.D. thanks the National Research Council for financial support.

- 
- [1] E. Yablonovitch, *Phys. Rev. Lett.* **58**, 2059 (1987).  
 [2] S. John, *Phys. Rev. Lett.* **58**, 2486 (1987).  
 [3] *Development and Applications of Photonic Band Gap Materials*, edited by C. M. Bowden, J. P. Dowling, and H. O. Everitt, special issue of *J. Opt. Soc. Am. B* **10** 279 (1993); *Photonic Band Structures*, edited by G. Kurizki and J. W. Haus, special issue of *J. Opt. Soc. Am. B* **19** (2002).  
 [4] M. Scalora, R. J. Flynn, S. B. Reinhardt, R. L. Fork, M. J. Bloemer, M. D. Tocci, J. Bendickson, H. Ledbetter, C. M. Bowden, J. P. Dowling, and R. P. Leavitt, *Phys. Rev. E* **54**, 2799 (1996).  
 [5] J. C. Maxwell, *A Treatise on Electricity and Magnetism* (Oxford University Press, Oxford, 1871).  
 [6] E. Nichols and G. F. Hull, *Ann. Phys.* **12**, 225 (1903).  
 [7] P. Mulser, *J. Opt. Soc. Am. B* **2**, 1814 (1985).  
 [8] M. I. Antonoyiannakis and J. B. Pendry, *Phys. Rev. B* **60**, 2363 (1999).  
 [9] M. L. Povinelli, M. Ibanescu, S. G. Johnson, and J. D. Joannopoulos, *Appl. Phys. Lett.* **85**, 1466 (2004).  
 [10] R. S. Tucker, D. M. Baney, W. V. Sorin, and C. A. Flory, *IEEE J. Sel. Top. Quantum Electron.* **8**, 88 (2002).  
 [11] J. D. Jackson, *Classical Electrodynamics*, 2nd ed. (Wiley, New York, 1975).  
 [12] H. Minkowski, *Nachr. Ges. Wiss. Goettingen, Math.-Phys. Kl.*, 53 (1908); H. Minkowski, *Math. Ann.* **68**, 472 (1910).  
 [13] M. Abraham, *Rend. Circ. Mat. Palermo* **28**, 1 (1909).  
 [14] Y. N. Obukhov and F. W. Hehl, *Phys. Lett. A* **311**, 277 (2003).  
 [15] R. Loudon, *J. Mod. Opt.* **49**, 821 (2002); R. Loudon, S. M. Barnett, and C. Baxter, *Phys. Rev. A* **71**, 063802 (2005).  
 [16] M. Mansuripur, *Opt. Express* **12**, 5375 (2004).  
 [17] Abraham [13] argued that in order to properly take into account the self force of an oscillating charge (radiation reaction), the first term of Eq. (5) must also be electromagnetic in nature. An extended discussion and a reproduction of these arguments are found in Ref. [11], and also reported in H. A. Lorentz, *Theory of Electrons* (Dover, New York, 1952).  
 [18] J. P. Gordon, *Phys. Rev. A* **8**, 14 (1973).  
 [19] V. G. Veselago, *Sov. Phys. Usp.* **10**, 509 (1968); J. B. Pendry, *Phys. Rev. Lett.* **85**, 3966 (2000).  
 [20] G. D'Aguanno, N. Akozbek, N. Mattiucci, M. Scalora, M. J. Bloemer, and A. M. Zheltikov, *Opt. Lett.* **30**, 1998 (2005).  
 [21] M. Scalora, G. D'Aguanno, N. Mattiucci, M. J. Bloemer, J. W. Haus, and A. M. Zheltikov, *Appl. Phys. B* **81**, 393 (2005); M. Scalora, M. Syrchin, N. Akozbek, E. Y. Poliakov, G. D'Aguanno, N. Mattiucci, M. J. Bloemer, and A. M. Zheltikov, *Phys. Rev. Lett.* **95**, 013902 (2005).  
 [22] M. Scalora, G. D'Aguanno, N. Mattiucci, N. Akozbek, M. J. Bloemer, M. Centini, C. Sibilina, and M. Bertolotti, *Phys. Rev. E* **72**, 066601 (2005).  
 [23] M. Scalora, N. Mattiucci, G. D'Aguanno, M. Larciprete, and M. J. Bloemer, *Phys. Rev. E* **73**, 016603 (2006).  
 [24] *Handbook of Optical Constants of Solids*, edited by E. D. Palik (Academic, New York, 1985).  
 [25] G. H. Liveness, *The Theory of Electricity* (Cambridge University Press, Cambridge, 1918); D. G. Lahoz and G. M. Graham, *J. Phys. A* **15**, 303 (1982).